JOURNAL OF AIRCRAFT
Vol. 50, No. 3, May–June 2013

Spanwise Variation in Circulation and Drag of Wings at Moderate Reynolds Number

S. L. Yang* and G. R. Spedding†
University of Southern California, Los Angeles, California 90089-1191

DOI: 10.2514/1.C031981

The measurement and prediction of the aerodynamic performance of airfoils and wings at chord Reynolds numbers below 10^5 are both difficult and increasingly important in the application to small-scale aircraft. Not only are the aerodynamics strongly affected by the dynamics of the unstable laminar boundary layer, but the flow is decreasingly likely to be two-dimensional as the Reynolds number decreases. The spanwise variation of the nominally two-dimensional flow along a two-dimensional geometry is often held to be responsible for the large variations in the measured profile drag coefficient c_d at this scale. Here, local two-dimensional drag coefficients are measured along a finite wing using nonintrusive particle image velocimetry methods. Variations in $c_d(y)$ can be related to local flow variations on the wing itself. Integrated values can then be compared with direct force balance data, and the dynamical significance of spanwise variability will be reevaluated.

Nomenclature

AR	=	aspect ratio
b	=	wing half-span, m
c	=	chord, m
C_D	=	total drag coefficient on a finite wing
c_d	=	sectional profile drag coefficient
$C_{D,i}$	=	induced drag coefficient on a finite wing
$C_{D,i,\mathrm{FB}}$	=	induced drag coefficient on a finite wing calculated from force balance measurements
$c_{d,\mathrm{PIV}}$	=	sectional profile drag coefficient obtained from particle image velocimetry measurements
$C_{D,\mathrm{PIV+FB}}$	=	total drag coefficient on a finite wing obtained by combining force balance and particle image velocimetry measurements
$C_{D,0}$	=	minimum total drag coefficient on a finite wing
$C_{d,0}$	=	minimum total drag coefficient on an infinite wing
C_f	=	laminar skin friction coefficient
C_L	=	total lift coefficient on a finite wing
c_s	=	separation line location, m
D'	=	drag per unit span, N/m
e_i	=	inviscid span efficiency
e_v	=	viscous span efficiency
f	=	body force, N
l	=	vertical transect in the wake region of the wing
n	=	normal vector to surface
p	=	pressure, $\mathrm{N/m^2}$
p_0	=	freestream pressure, $\mathrm{N/m^2}$
q	=	dynamic pressure, $\mathrm{N/m^2}$
Re	=	Reynolds number
S	=	control surface around the wing
$\mathbf{U}$	=	mean velocity vector, m/s
U	=	mean component of velocity in x, m/s
U_0	=	freestream velocity, m/s
x, y, z	=	coordinates are streamwise, spanwise, and normal directions
α	=	angle of attack, deg
$\Delta*$	=	variation
δ	=	boundary-layer thickness, m
θ	=	momentum integral, m
σ	=	standard deviation
Ω	=	normalized vorticity
$\boldsymbol{\omega}$	=	vorticity vector, rad/s
ω_y	=	spanwise component of vorticity, rad/s
$\langle * \rangle$	=	root-mean-square value
$\bar{*}$	=	time-averaged value

I. Introduction

STANDARD airfoil performance data do not often extend beneath $Re \approx 100,000$, and when they do, there are large discrepancies between the studies of airfoils under ostensibly the same conditions [1,2]. In the range $30,000 \leq Re \leq 100,000$ in particular, there is a heightened sensitivity to small variations in the geometry and operating conditions. Gross performance parameters depend strongly on the initial laminar boundary-layer stability and separation, transition to turbulence of the separated shear layer, and possible subsequent reattachment in some time-averaged sense. Though practical wings are finite in span, those of moderate aspect ratio share many of the characteristics that have been demonstrated for two-dimensional (2-D) airfoil sections [3], as the central part of the wing sees little influence from the tip vortices. One of the well-known characteristics that has not been measured for the finite wing, however, is the possible variation in the sectional drag coefficient as measured from wake surveys [1,4]. At these Reynolds numbers, wake surveys and calculating drag components pose particular problems (described next), and it is not known whether the variations will be large or whether they could be responsible for discrepancies or variations in force measurement. The purpose of this paper is to carefully document the spanwise variation in the measured sectional drag coefficient in experiments that combine optical flow measurement techniques with direct force balance data from custom instrumentation with adequate resolution of the small forces involved at these Reynolds numbers. We may then determine whether quasi-2-D analysis is sufficient (or where it is sufficient) and then compare the variations with the previously reported variations on 2-D geometry. Ultimately, the findings will extrapolate out to small unmanned air vehicles with fixed wing design.

A. Drag Variation at Transitional Reynolds Numbers

Although much literature exists for the Eppler 387 [4], an airfoil commonly used on sailplanes and gliders, the agreement of the measured lift and drag coefficients among different facilities deteriorates as the Reynolds number decreases, as seen in Fig. 1. At $Re = 60,000$, Δc_d is large, and although turbulence levels, acoustic

Received 30 May 2012; revision received 27 August 2012; accepted for publication 3 December 2012; published online 18 April 2013.

*Department of Aerospace and Mechanical Engineering; shanling.yang@usc.edu. Member AIAA.

†Professor, Department of Aerospace and Mechanical Engineering; geoff@usc.edu. Member AIAA.

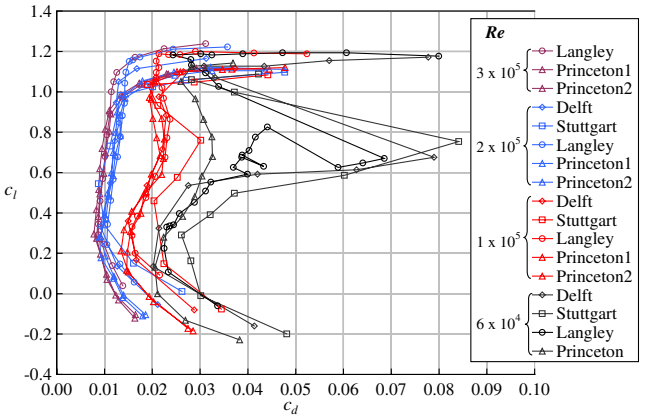

Fig. 1 Drag polars for the 2-D Eppler 387 at various Reynolds numbers from different facilities replotted from [5].

noise, model accuracy, and physical vibrations may contribute to these measured drag discrepancies, it has also been suggested that spanwise drag variation is responsible [4]. This is partly because measurements of relatively small drag forces are usually made not by direct measurement on the wing but by integrating velocity/pressure information from scanning or arrayed sets of pitot tubes in the wake, when the sampling of spatially inhomogeneous data can be incomplete. Moreover, precisely at these low Reynolds numbers, the validity of the method has been questioned due to the upstream influence of wake rakes on the flow.

The spanwise drag variation $c_d(y)$ of an E374 wing section has been measured at various angles of attack α and downstream locations x/c for $Re = 200,000$ (Fig. 2) [1]. Figure 2 shows that, although the variation is most pronounced at the furthest downstream locations, all stations vary across the span, and the variation is spread across the entire span. The total drag estimates would have to come from a number of span stations, and one may imagine cases in which it could be wrongly estimated if the measurement stations coincided with peaks or troughs. Most routine c_d measurements are taken at some x/c (=2.25 for [1]) in which the pressure gradients are small, and the local flow is mostly parallel to the tube array. Indeed, for drag calculations made from pitot-static pressure measurements, a proper downstream wake survey location has been shown to be a function of the drag formulation equations themselves [6]. Steady-state equations have been shown to be applicable for survey regions sufficiently far downstream so that there is negligible variation in static pressure [6,7], but this is where the spanwise variation in Fig. 2 is most pronounced. Finally, the larger variations in c_d in Fig. 1 are for $Re < 100,000$, and it is not clear how to extrapolate the results at $Re = 200,000$ in Fig. 2 to this regime, in which apparently the flow properties are much less predictable.

B. Drag Calculations

The momentum equations for a viscous flow in Einstein notation are

$$\rho\frac{\partial \tilde{u}_i}{\partial t} + \rho\tilde{u}_j\frac{\partial \tilde{u}_i}{\partial x_j} = -\frac{\partial \tilde{P}}{\partial x_i} + \rho f_i + \mu\frac{\partial^2 \tilde{u}_i}{\partial x_j \partial x_j} \tag{1}$$

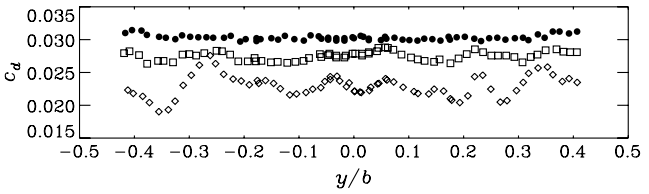

Fig. 2 $c_d(y)$ of an E374 wing section at $Re = 200{,}000$, $\alpha = -6.4$ at $x/c = 1.0$ (trailing edge) (solid circles), $x/c = 1.7$ (squares), and $x/c = 2.23$ (diamonds) replotted from [1].

where $\tilde{u}_i$ is the total instantaneous velocity composed of the mean, U_i, and fluctuating, u_i, parts ($\tilde{u}_i = U_i + u_i$);$\tilde{P}$ is the total pressure also composed of mean and fluctuating parts ($\tilde{P} = P + p$); ρ is the density of the fluid; μ is the dynamic viscosity; f is the total body force per unit mas; and $i, j = (x, y, z)$. For our wing model system, x is streamwise, y is spanwise, and z is normal to the chord c and span b when the wing is at $\alpha = 0$ deg. Equation (1) can alternatively be written by decomposing it into the mean and fluctuating velocity components to yield the Reynolds-averaged Navier–Stokes equation:

$$\rho\frac{\partial U_i}{\partial t} + \rho U_j\frac{\partial U_i}{\partial x_j} = -\frac{\partial P}{\partial x_i} + \rho f_i + \mu\frac{\partial^2 U_i}{\partial x_j \partial x_j} - \rho\frac{\partial}{\partial x_i}\overline{u_i u_j} \tag{2}$$

where $\overline{u_i u_j}$ is the Reynolds stress tensor. In classical aeronautics applications, the flow around a fixed wing in steady motion is assumed to be steady and inviscid. Furthermore, if a region of flow is surveyed far from the body, then the pressure there can be assumed to be equal to the constant, undisturbed freestream pressure p_0, and the turbulent motion of the flow is negligible. With these additional constraints, the time derivative term on the left side of Eq. (2), the pressure term, and the last two terms on the right side drop out, leaving

$$\rho U_j\frac{\partial U_i}{\partial x_j} = \rho f_i \tag{3}$$

Equation (3) relates the body force in any direction with the mean momentum flux in that direction. It is then convenient to express this relationship in integral form so that the forces in one region can be related to the fluxes through an enclosing control volume with surface area S and corresponding normal vector n, and so

$$\int_S \rho U_i U_j n_j \,\mathrm{d}S = \int_S \rho f_i \,\mathrm{d}S \tag{4}$$

The component of the force in the streamwise direction f_x can therefore be calculated from the change in momentum flux between the upstream and downstream surfaces, and when the flow and body geometry are uniform in one direction, such as the span, the drag force per unit span D' can be evaluated from just two line integrals:

$$D' = -\int_{l_1} \rho_1 U_1^2 \,\mathrm{d}z + \int_{l_2} \rho_2 U_2^2 \,\mathrm{d}z \tag{5}$$

where ρ_1 and U_1 are the density and velocity of the fluid upstream of the body at a vertical transect l_1, and ρ_2 and U_2 are the density and velocity downstream of the wing at l_2, which contains all of the wake region W. If $U_1 = U_0$ and ρ equals a constant, the total positive drag on the body with span b can be written as

$$D = \rho U_0^2 b\theta \tag{6}$$

where the momentum integral θ depends only on the variation of mean velocity components over W:

$$\theta = \int_W \left(\frac{U_2}{U_0} - \left(\frac{U_2}{U_0}\right)^2\right)\mathrm{d}z \tag{7}$$

The section profile drag coefficient c_d is then

$$c_d = \frac{2\theta}{c} \tag{8}$$

The drag formulation of Eqs. (4–8) differs slightly from other well-known methods in the literature [6,8–10]. The total drag formulation in [9] includes a total pressure loss term and allows for nonzero cross-plane velocity components, whereas Eqs. (4–8) are more restrictive, assuming that the wake is surveyed far enough downstream so that the downstream pressure is equal to the undisturbed pressure, and the turbulent flow is negligible (and so the average cross-plane velocity components go to zero). Betz's equation for the profile drag [8] takes

the survey location only in the wake of the body by introducing a fictitious velocity component that is nonzero only in the region of the viscous wake, whereas the current method does not use a fictitious velocity but rather takes the survey location far downstream. The equivalent equation for profile drag in [10] uses the total and static pressures measured close behind the body, whereas the current method only considers velocities measured at two locations (upstream and downstream of the body).

The total drag on a finite wing is commonly described as the sum of two components:

$$C_D = c_d + C_{D,i} \tag{9}$$

c_d is the profile drag coefficient in Eq. (8), which is a function of α, and can be expressed as

$$c_d = c_{d,0} + c_d(\alpha) \tag{10}$$

where $c_{d,0}$ is the minimum drag coefficient for a 2-D wing section. $C_{D,I}$ is the induced drag coefficient:

$$C_{D,i} = \frac{C_L^2}{\pi e_i \mathrm{AR}} \tag{11}$$

where C_L is the lift coefficient of a finite wing with aspect ratio AR, and $e_i \leq 1$ is the inviscid span efficiency factor, which accounts for departures from the ideal elliptic spanwise load distribution. It can be convenient and reasonable to write C_D as a quadratic function of C_L, and then a viscous span efficiency factor e_v, which can be obtained through the slope approximation of the C_D-C_L^2 curve [3], can be used to write the total drag coefficient as

$$C_D = C_{D,0} + \frac{C_L^2}{\pi e_v \mathrm{AR}} \tag{12}$$

where $C_{D,0}$ is the minimum drag value from the C_L-C_D polar. The slope values from the C_D-C_L^2 curves differ between 2-D airfoils and finite wings, as shown in [3], and so careful distinction between the two conditions must be made. Either of these two drag decomposition methods [using either Eqs. (9) and (11) or Eq. (12) alone] can be used to estimate the drag components that are essentially inviscid (induced drag due to downwash behind a lifting wing) and viscous (profile drag from skin friction and boundary-layer separation) in origin. Such a separation is simple at high Reynolds numbers but perhaps less easy to disentangle at moderate to low Reynolds numbers, when the behavior of the viscous boundary layer is so influential [11].

C. Objectives

This paper provides the first direct check on the spanwise variation of local c_d measurements on a smooth airfoil of moderate thickness for $Re < 100,000$. When and if variation is found, the associated instantaneous and time-averaged velocity fields on the wing can be checked for conditions that may cause the observed fluctuations. Direct association of the force coefficients with the relevant flowfield is still quite rare in aeronautics practice but is important in regimes with such a rich variety of important flow behavior. The local drag measurements come from particle image velocimetry (PIV)-derived velocity fields, and the total inferred and integrated drag on the wing can be compared with direct force balance measurements.

II. Materials and Methods

A. Experimental Setup

Experiments were performed in a closed-loop wind tunnel with an octagonal test section of wall to wall width 1.37 m and 5.7 m in the streamwise direction. The empty test-section turbulence level is 0.025% for spectral frequencies between $2 \leq f \leq 200$ Hz in the velocity range $5 \leq U \leq 26$ m/s. Flow uniformity measurements showed no more than 0.5% velocity deviation from the mean velocity for a given cross section [12]. The wing was machined from a solid aluminum block with AR = 5.8 (span $b = 52.7$ cm and chord $c = 9$ cm) with an Eppler 387 airfoil section, as shown in the Fig. 3 inset. All measurements were made at $Re = 30,000$, which is deliberately set to be in a region of $C_L(C_D)$ space in which abrupt switching between stable states can occur. Previous experimentation [12] on the same wing and same conditions shows that the flow separates before the trailing edge, and so small variations in the trailing-edge thickness were not a concern.

PIV was used to estimate velocity components (u, w) in the 2-D plane (x, z) (Fig. 3). A dual-head Continuum Nd–Yag laser was used to generate coplanar sheets in the smoke-seeded flow in the test section. Paraffin-based particles were generated with a Colt 4 smoke machine. The laser sheets were oriented in the x-z plane across the tunnel, illuminating single chordwise span stations on the wing or downstream of it. A Kodak ES 1.0 CCD camera with 1008×1018 pixels and an 85-mm-focal-length lens was placed above the wind tunnel and traversed in the spanwise direction in concert with the scanned laser sheet and acquired images. The time between laser pulses was set to a nominal 260 μs. Images were taken at 35 span stations spaced 1 cm apart at three streamwise locations (Fig. 3) and at six angles of attack, $\alpha = 0, 2, 4, 6, 8, 10$ deg.

B. Spanwise Vorticity Measures

Persistent features in the time-averaged wake profiles can be traced upstream to the generating conditions on the wing, in which the separation line location and spanwise vorticity magnitudes in the separation region can be related to the wake structure. Contrasting regions of interest were studied for the $\omega_y(x, z)$ measurements at two angles of attack. For $\alpha = 0$ deg, where the majority of the flow across the top surface of the wing is still attached, the regions of interest were the fore- and aft-attached regions, denoted by "a" and "b" in Fig. 4a. Region a encompassed the front (windward) half of the airfoil, following the boundary points along the top surface of the airfoil and extending to a height that enclosed the entire boundary-layer profile. Region b covered the back (leeward) half of the airfoil with the same height as region a. Statistics from these two regions were collected separately.

When the separation line has moved forward by a significant fraction of the chord, such as at $\alpha = 8$ deg, the regions of interest were the attached region and the separated region, "a" and "s", in Fig. 4b. The attached region was the same as region a for $\alpha = 0$ deg. The separated region was defined by a triangle from midchord to the trailing edge (Fig. 4b).

For all PIV images at a given span station and region of interest, $i(a, b, s)$, the root mean square of the instantaneous spanwise component of vorticity ω_y values were calculated over that region to give a single rms vorticity value, $\langle \omega_y \rangle_i$:

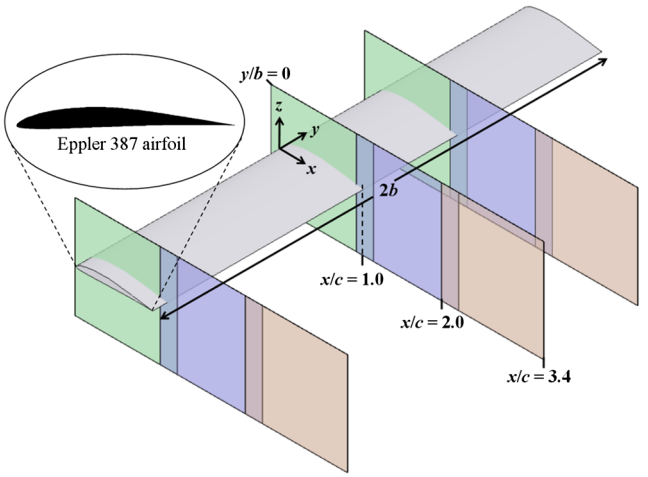

Fig. 3 Three streamwise locations and three (of 35) spanwise stations at which PIV images were taken. The coordinate system origin is the leading edge at midspan. The trailing edge is $x/c = 1.0$. Inset: E387 profile.

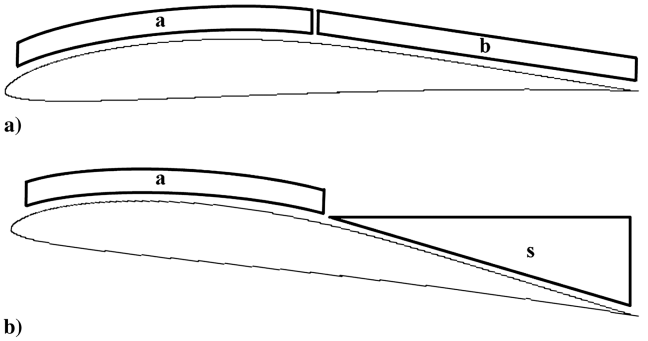

Fig. 4 Regions of interest for spanwise vorticity fields. Top: $\alpha = 0$ deg fore, a, and aft, b. Bottom: $\alpha = 8$ deg attached, a, and separated, s.

$$\langle \omega_y \rangle_i = \sqrt{\frac{1}{N}\sum_{k=1}^{N} (\omega_y(\{x,z\} \in i))_k^2} \tag{13}$$

where N is the total number of images. $\langle \omega_y \rangle_i$ was then normalized by the chord and mean velocity and is denoted

$$\langle \Omega \rangle_i = \frac{\langle \omega_y \rangle_i c}{U} \tag{14}$$

The location of the separation point itself can be measured directly and independently from raw particle images. At values of α for which separation occurs on the front half of the wing ($0.0 \le x/c \le 0.4$), the separation line is visible as a thin dark line. In this line, fluid has come directly from the boundary layer where fewer tracer particles (introduced in the exterior flow) have penetrated. c_s is the chordwise location of this separation line.

C. Force Balance

Lift and drag forces were measured with a custom cruciform-shaped force balance (described in [12,13]), placed below the wind-tunnel floor. The force balance was capable of measuring the lift, drag, and pitching moment. Measurements were averaged over 9000 samples at a sample rate of 1000 Hz. Careful calibration procedures were performed each day before data acquisition; static calibrations were performed from 0 to 360 mN in 4 mN steps at different moment arms. The force balance measurement has an expected uncertainty of 1 mN. The expected friction drag on a flat plate of the same size as the E387 wing at zero degrees of incidence is approximately 11 mN. In force balance measurements, α was varied from -10 to 20 deg in steps of 1 deg. Three tests were performed for both increasing and decreasing α, and results were averaged.

The force balance measures the total drag (which will be labeled $C_{D,\mathrm{FB}}$) as well as lift, C_L. The profile drag values at the six different angles of attack are obtained from the PIV measurements of the momentum wake defect in the midsection of the wing ($-0.4 \le y/b \le 0.4$); this profile drag component will be labeled $c_{d,\mathrm{PIV}}$. The span efficiency [Eqs. (11) and (12)] for the E387 wing is initially unknown, and so $C_{D,i,\mathrm{FB}}$ can be estimated by subtracting $c_{d,\mathrm{PIV}}$ from $C_{D,\mathrm{FB}}$ at each α. Because C_L is known at each α, a least-squares fit for $C_{D,i,\mathrm{FB}}$ values can be used to solve for e_i and e_v from Eqs. (11) and (12). The total drag achieved by adding $c_{d,\mathrm{PIV}}$ and $C_{D,i,\mathrm{FB}}$ with the calculated efficiency values will be labeled $C_{D,\mathrm{PIV+FB}}$ and is necessarily equal to $C_{D,\mathrm{FB}}$. The uncertainties in $C_{D,i,\mathrm{FB}}$ derive primarily from the standard deviation in C_L from force balance measurements, and the uncertainties in $c_{d,\mathrm{PIV}}$ are obtained by methods explained in the following section.

III. Results

A. Spanwise Drag Variation at Moderate Reynolds Numbers

Correct estimates of c_d from Eq. (10) require that converged time-averaged profiles exist and that contributions from $\mathrm{d}p/\mathrm{d}x$ are negligible. This condition occurs at some distance downstream, estimated to be $x/c > 3$ for similar conditions [14]. Mean profile integrals $\int_W U_2(z)\,\mathrm{d}z$, where W is a domain in z where the wake defect exists, converged to within 13% after 120–210 image pairs, depending on α. Satisfactory convergence of $\theta(x)$ can be claimed after $x/c = 2.75$, and all subsequent data use streamwise averages over $x/c \in [3.0, 3.4]$.

The results of integrating Eq. (7) to obtain $\theta(y)$ at the six different angles of attack at the downstream location $x/c = 3.4$ yield $c_d(y)$ for the E387 wing at $Re = 30,000$, shown in Fig. 5. There is increasing variation near the wingtip ($y/b = -1.0$) with increasing α, which is mostly a consequence of the nonzero mean out-of-plane momentum flux. There is also measurable variation over the midportion of the wing between $-0.4 \le y/b \le 0.4$ where the variation with y in c_d is higher than the measurement uncertainty. $c_d(y_0)$ increases as α increases, but there is no obvious variation in the absolute magnitude of Δc_d with α in the wing center. Because the wingtip effects are incidental to the main focus here, they are not analyzed further, and the resulting focus will be on the midportion of the wing.

The momentum thickness θ was obtained by several methods, including averaging different numbers of image pairs to obtain $U(z)$, applying different interpolation methods to acquire the boundaries for the momentum defect regions, and using different integration methods to calculate θ from a given mean profile The uncertainty Δc_d is the maximum difference in c_d values obtained using these various methods. The greatest relative variation in c_d in the midsection of the wingspan ($-0.4 \le y/b \le 0.4$) is 27% at $\alpha = 0$ deg. By definition, in this procedure, any measured variation must come from systematic and repeatable variations in the profile amplitude and width.

If there is variation in average values of θ and c_d due to time-averaged variation in flowfield, then it should be possible to trace such variations upstream. $c_d(y)$ at $\alpha = 0$ deg and $\alpha = 8$ deg is compared at two different downstream locations, $x/c = 3.4$ and 2.0 (Fig. 6).

At $\alpha = 0$ deg, the pattern of the above-threshold spanwise $c_d(y)$ variation matches for the two x/c locations. The difference between

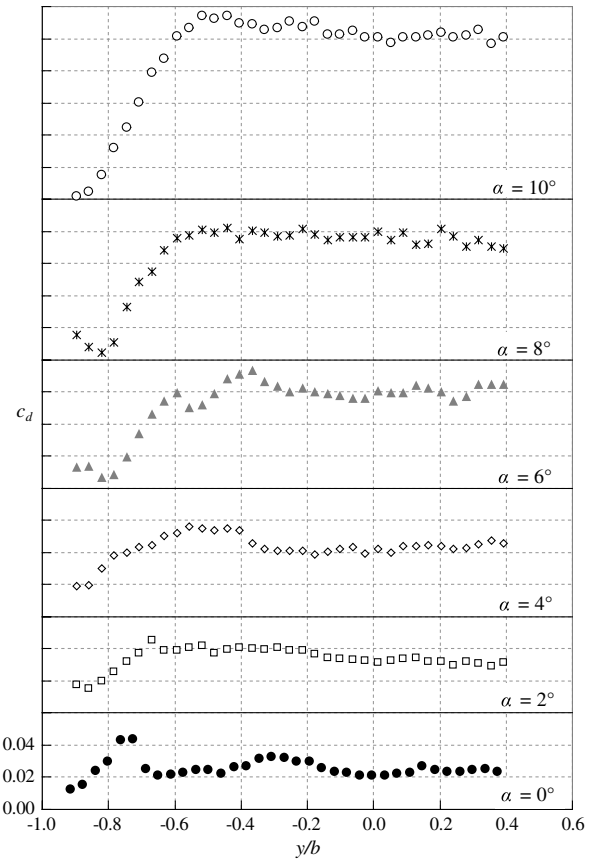

Fig. 5 $c_d(y)$ at $\alpha = 0, 2, 4, 6, 8, 10$ deg. The symbol size is chosen to match the size of the measurement uncertainty.

the two sets of data is a slight offset (the calculated drag values are slightly higher further downstream). At $\alpha = 8$ deg, the correlation is less obvious, but there are correlated variations, significantly above noise, that are coherent in x. If the correlations in the wake are coherent in x, then it may be possible to trace their origin back to conditions on the wing.

B. Spanwise Vorticity and Separation Point Location Variation

At $\alpha = 0$ deg, the instantaneous and time-averaged ω_y look similar as the flow is steady and laminar separation occurs shortly before the trailing edge (Figs. 7a and 7b). At $\alpha = 8$ deg, the flow separation is earlier, and the separated shear layer has become unstable, generating coherent structures that impinge upon the downstream portion of the suction surface. Consequently, ω_y and $\bar{\omega}_y$ are not the same (Figs. 7c and 7d). The earlier separation of the boundary layer is associated with increased turbulent levels in the separated region and reduced aerodynamic performance. At $x \approx 10$ mm, $Re_x \approx 3300$, and the boundary-layer thickness $\delta = \frac{5.2x}{\sqrt{Re_x}} \approx 0.9$ mm. The grid resolution is 1.5 mm, and so the laminar boundary layer is not resolved. The boundary-layer vorticity and the possible presence of small separation and reattachment regions upstream of the trailing-edge separation are therefore not accessible to this experiment. However, the statistics of the larger separated region can be used as indicators of variation in the separation point and conditions behind it.

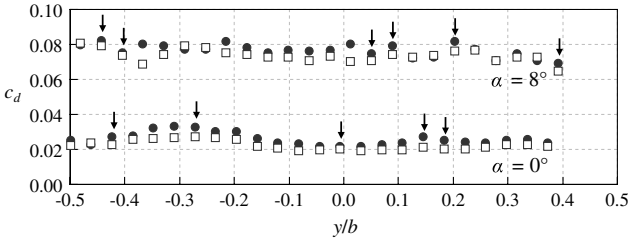

Fig. 6 $c_d(y)$ **at** $\alpha = 0$ **and 8 deg at** $x/c = 3.4$ **(solid circles) and** $x/c = 2.0$ **(squares). The symbol size matches the measurement uncertainty. Arrows denote data points in subsequent sections.**

At $\alpha = 0$ deg, five y/b stations in the midportion of the wing ($-0.5 \le y/b \le 0.5$) were chosen, in which $c_d(y)$ varied similarly at $x/c = 3.4$ and $x/c = 2.0$ (indicated by arrows in Fig. 6). $\langle\Omega\rangle_{a,b}$ are shown at the different span stations in Fig. 8. $\langle\Omega\rangle_a$ varies with the resolved outer boundary-layer vorticity over the attached part of the airfoil and is therefore a measure of the strength of the bound vorticity on the wing. $\langle\Omega\rangle_a$ may be expected to vary with the lift coefficient but may not be sensitive to changes in drag. When flow separation is mild, $\langle\Omega\rangle_b$, which averages all spanwise vorticity over the aft surface, has a lower magnitude (the mean boundary layer has thickened) but still has very similar variation. Neither $\langle\Omega\rangle_a$ nor $\langle\Omega\rangle_b$ varies significantly across the span or in phase with $c_d(y)$. Apparent variations in phase with variation in $c_d(y)$ do not rise above the measurement uncertainty. Flow separation does not occur until close to the trailing edge at $\alpha = 0$ deg, and so there is no separated region along the top of the wing as in the case of higher α.

At $\alpha = 8$ deg, six y/b stations were also chosen in which $c_d(y)$ varied similarly at $x/c = 3.4$ and $x/c = 2.0$ (indicated by arrows in Fig. 6). $\langle\Omega\rangle_{a,s}$ and c_s/c are shown at the different span stations in Fig. 9. $\langle\Omega\rangle_s$ varies as c_d, showing, unsurprisingly, that a high local c_d is associated with high turbulence levels over the trailing half-chord. There is no clear correlation of $\langle\Omega\rangle_a$ with c_d. c_s varies inversely with $\langle\Omega\rangle_s$, and so high turbulence in the separation region is associated with earlier separation and higher local c_d.

C. Force Balance

In Fig. 10, $C_{D,\mathrm{FB}}$ is compared with values calculated from the wake measurements that use $C_{D,i}$ and the least-squares fit on e_i [Eq. (11)] to match the sum of $C_{D,i}$ and $C_{D,\mathrm{PIV+FB}}$. The best fit yielded $e_i = 0.83$. This estimate uses the wake-measured variation of $c_d(\alpha)$ to estimate the profile drag. An alternative is to use the force balance data to calculate the constant value of $C_{D,0}$ (also sometimes known as the profile drag), and then the implicit variation of c_d with C_L^2 is included in the value of the viscous span efficiency e_v, which can again be estimated by least-squares regression of $C_{D,\mathrm{PIV+FB}}$ on α. The fit is satisfactory when $e_v = 0.3$ (Fig. 11) [3]. This estimation by least-squares regression essentially yields values of e_v and e_i that would otherwise be obtained through a linear fit and slope calculation of the C_D-C_L^2 curve. The estimated slope at low α is 0.14, compared with 0.09 for a different E387 wing at the same Reynolds number in [3], in

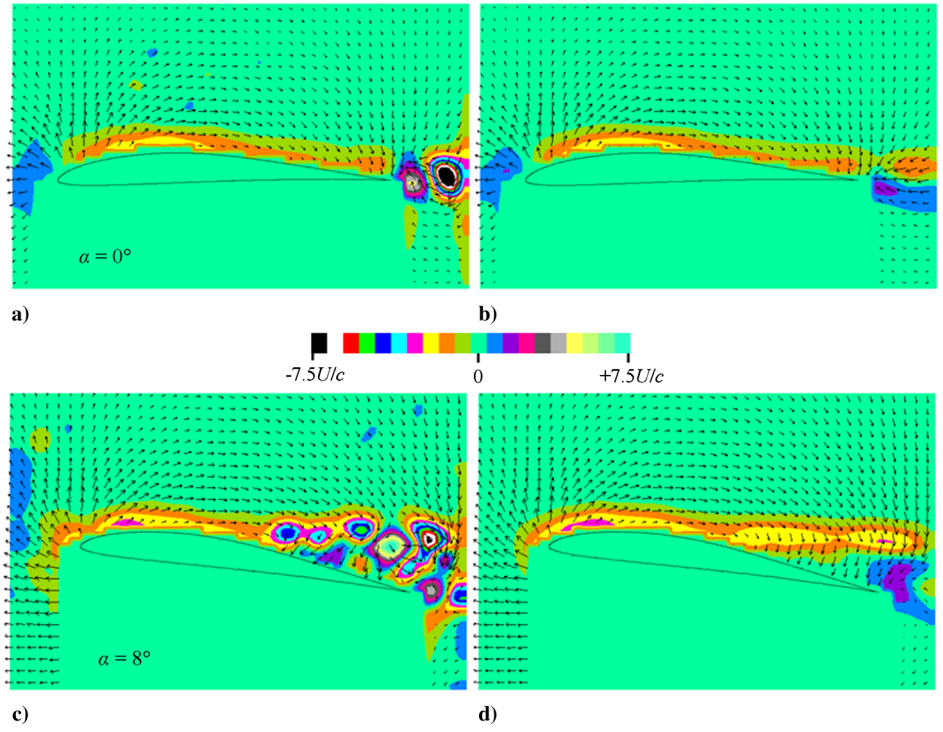

Fig. 7 (a) $\omega_y(x,z)$ **and** (b) $\bar{\omega}_y(x,z)$ **at** $\alpha = 0$ **deg;** (c) $\omega_y(x,z)$ **and** (d) $\bar{\omega}_y(x,z)$ **at** $\alpha = 8$ **deg. Arrows are fluctuating velocity vectors.**

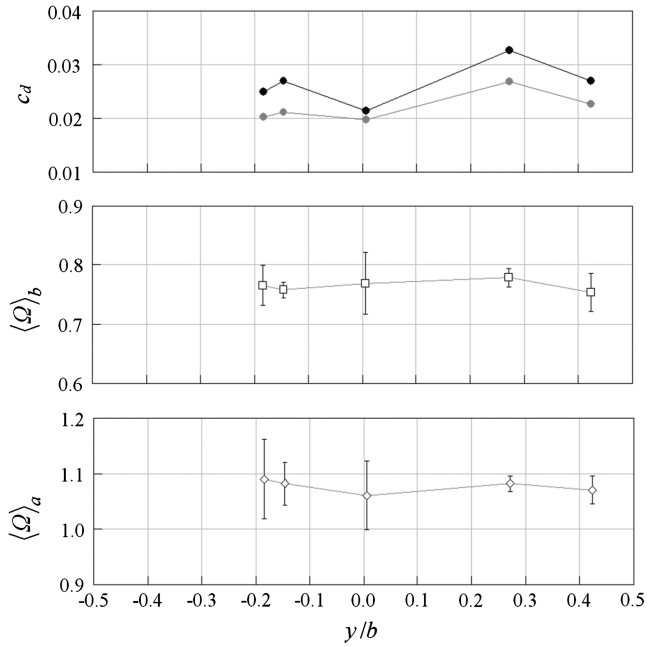

Fig. 8 Spanwise $c_d(y)$ (top: $x/c = 3.15$ in black; $x/c = 1.75$ in gray), $\langle\Omega\rangle_b$ (middle), and $\langle\Omega\rangle_a$ (bottom) at $\alpha = 0$ deg.

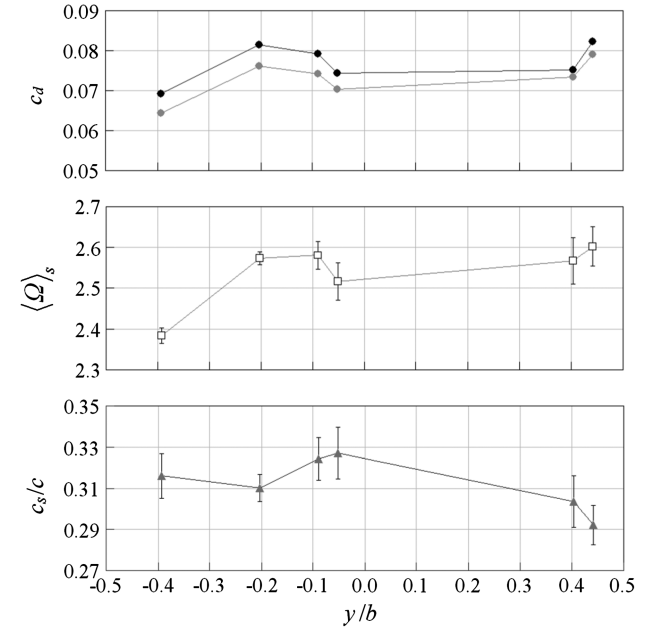

Fig. 9 Spanwise $c_d(y)$ (top: $x/c = 3.15$ in black; $x/c = 1.75$ in gray), $\langle\Omega\rangle_s$ (middle), and $\langle\Omega\rangle_a$ (bottom) at $\alpha = 8$ deg.

which it was noted that such values have limited significance when the lift–drag polars themselves have shapes very different from model assumptions.

IV. Discussion

There is measurable variation in $c_d(y)$ on the E387 wing at $Re = 30,000$ over all the tested $\alpha(0 \le \alpha \le 10$ deg). The large differences in the measured $c_d(y)$ between the midspan and the wing tip (up to 98% at $\alpha = 10$ deg for $0.0 \le y/b \le 0.9$) are related to the nonnegligible momentum flux in the out-of-plane directions and are related directly to the lift on the finite wing. However, spanwise $c_d(y)$ variation also occurs in the midportion of the wing (up to 27% variation at $\alpha = 0$ deg for $0.0 \le y/b \le 0.2$), in which the local flow may otherwise be considered to be close to two dimensional.

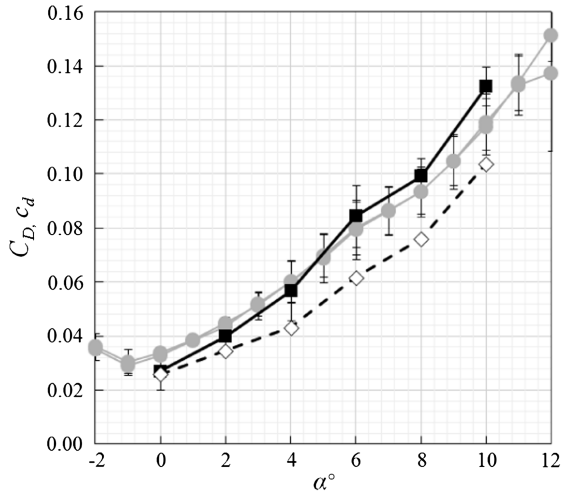

Fig. 10 Combined force balance and PIV drag results. $C_{D,\mathrm{FB}}$ (gray line + circles), $c_{d,\mathrm{PIV}}$ (dashed line + diamonds), $C_{D,\mathrm{PIV+FB}}$ using $e_i = 0.83$ (solid line + squares).

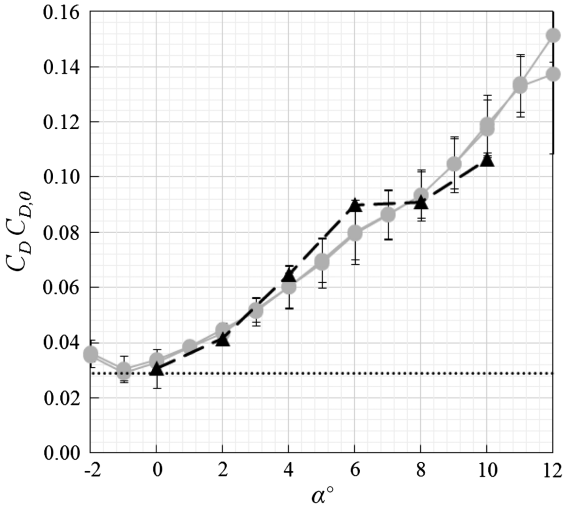

Fig. 11 $C_{D,\mathrm{FB}}$ (gray line + circles), $C_{D,0}$ (dotted line), $C_{D,\mathrm{PIV+FB}}$ using $e_v = 0.3$ (dashed line + triangles).

The $c_d(y)$ variation trends are preserved at different x/c locations, and tracing the flow back to the on-wing conditions shows that, at $\alpha = 8$ deg, in which significant flow separation occurs, $\langle\Omega\rangle_s$ variation is directly proportional to $c_d(y)$ variation. This was not the case for $\langle\Omega\rangle_a$ or at $\alpha = 0$ deg, in which separation does not occur until near the trailing edge. The fore–aft movement of the separation point location showed that an increase in $\langle\Omega\rangle_s$ corresponds to earlier separation, suggesting that, at high α, the location of the separation line c_s is not uniform and two dimensional. The location of separation affects the size of the separated region above the airfoil, as measured by the magnitude of the spanwise vorticity in the separated region, and correlates with the wake momentum deficit, and hence the local sectional drag, and its measurement.

The results of the $c_d(y)$ variation study at $Re = 30,000$ are quantified by the same normalization procedure as described in Sec. I.B. and compared with the literature results [1,4] in Fig. 12. Although the values of drag variation are associated with two different Reynolds numbers and two different (but similar) airfoils, both show a local maximum at $\alpha \sim 6$ deg, which is where the separation location is highly sensitive to small disturbances. The lower-Reynolds-number data show that the relative variation increases

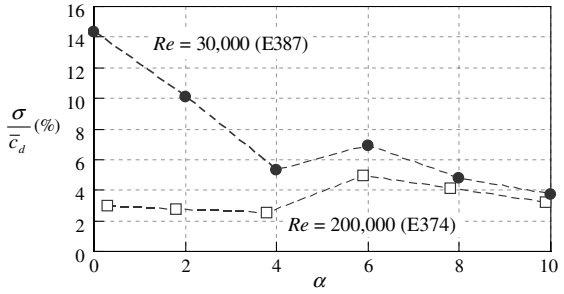

Fig. 12 σ at $Re = 200{,}000$ for the E374 from [1] (squares) and $Re = 30{,}000$ for the E387 from the current study (solid circles).

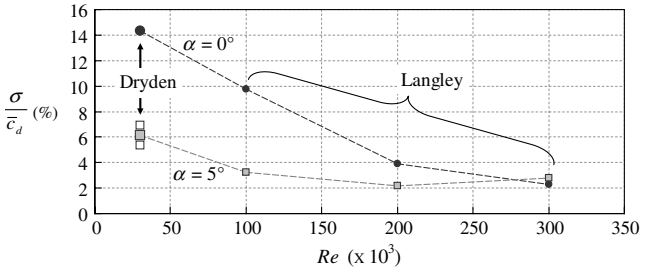

Fig. 13 $\frac{\sigma}{\bar{c}_d}$ at $\alpha = 0$ (solid circles) and 5 deg (gray squares) at various Reynolds numbers from Langley [4] and Dryden. The value at $\alpha = 5$ deg from Dryden is an average of the values at $\alpha = 4$ (bottom white square) and 6 deg (top white square).

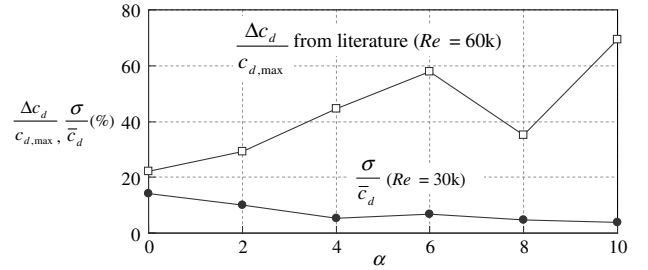

Fig. 14 Drag variation from different facilities (squares) and spanwise $c_d(y)$ from current study (solid circles).

for small α. The variation of c_d with y is much higher in current experiments, but that is because the Reynolds number is lower.

The variation magnitude is shown as a function of Reynolds number in Fig. 13. Clearly, σ decreases as the Reynolds number increases, but the increase in $\sigma/\bar{c}_d$ with decreasing Reynolds number is consistent in both facilities.

Finally, σ for the current study at $Re = 30{,}000$ is compared with Δc_d among different facilities at $Re = 60{,}000$ in Fig. 14. For $0 \le \alpha \le 10$ deg, σ at $Re = 30{,}000$ is less than Δc_d at $Re = 60{,}000$. Figure 13 shows that drag variation increases as the Reynolds number decreases, and so σ at $Re = 60{,}000$ will be lower still than at $Re = 30{,}000$. The observed $c_d(y)$ variation is much less than the drag variation from the literature at $Re = 60{,}000$, and therefore, $c_d(y)$ variation is not the main cause of the discrepancies in the measured c_d among different facilities.

The separation of drag into its different components is achievable at $Re = 30{,}000$ if e_i and e_v are determined empirically. Because only the α-dependent profile drag c_d is obtained from the PIV-based measurements, a second method (in this case, direct force balance measurements) must be used to complete the drag measurement/calculation, which involves two unknowns, e and $C_{D,i}$. At $Re = 30{,}000$, the drag measurements imply values of e_i and e_v of 0.83 and 0.3, respectively, which are very low compared with the usual high-Re default values close to 1 but in agreement with previous findings at moderate Reynolds numbers [3]. The existence of persistent spanwise variation in the wake defect magnitude, and hence c_d, along the span supports the argument that a single parameter description of the departure from ideal uniform conditions may not be a very good reflection of the detailed flowfield on the wing.

V. Conclusions

At transitional Reynolds number flows, particularly in the subregime $30{,}000 \le \mathrm{Re} \le 70{,}000$, the drag values reported by various facilities for smooth airfoils, including the E387, differ significantly, and it has been suggested that spanwise drag variation is one possible cause of these disparities. Airfoil/wing performance, especially at low Reynolds numbers, is extremely sensitive to separation location, and variations in separation location do indeed correlate with variations in the local measured sectional drag coefficients. However, the magnitude of these variations in the nominally two-dimensional center section of the wing reported here is small and is thus unlikely to account for the differences in reported results among different facilities.

Acknowledgments

This research was supported through a National Science Foundation fellowship. The authors wish to thank Gauri Kahnolkar for her assistance in data acquisition and processing, as well as the rest of the students in the Dryden Wind Tunnel team for their support: Austin Reed, Vaasu Swaminathan, Rob Rovai, Travis Metzger, Aditya Vaidyanathan, and Keith Holmlund.

References

[1] Guglielmo, J. J., and Selig, M. S., "Spanwise Variations in Profile Drag for Airfoils at Low Reynolds Numbers," *Journal of Aircraft*, Vol. 33, No. 4, 1996, pp. 699–707. doi:10.2514/3.47004

[2] Simons, M., *Model Aircraft Aerodynamics*, 4th ed., Special Interest Model Books, Poole, England, U.K., 1999, pp. 227–259.

[3] Spedding, G. R., and McArthur, J., "Span Efficiencies of Wings at Low Reynolds Numbers," *Journal of Aircraft*, Vol. 47, No. 1, 2010, pp. 120–128. doi:10.2514/1.44247

[4] McGhee, R. J., Walker, B. S., and Millard, B. F., "Experimental Results for the Eppler 387 Airfoil at Low Reynolds Numbers in the Langley Low-Turbulence Pressure Tunnel," NASA TM-4062, 1988, pp. 25–26.

[5] Selig, M. S., Guglielmo, J. J., Broeren, A. P., and Giguere, P., *Summary of Low-Speed Airfoil Data*, Vol. 1, Soar Tech Publ., Virginia, Beach, 1995, pp. 19–20.

[6] Takahashi, T. T., "On the Decomposition of Drag from Wake Survey Measurements," AIAA Paper 97-0717, Jan. 1997.

[7] Taylor, G. I., "The Determination of Drag by the Pitot Traverse Method," Aeronautical Research Council, Rept. R&M-1808, London, 1937.

[8] Betz, A., "A Method for Direct Determination of a Wing Section Drag," NACA TM-No. 337, 1925.

[9] Bollay, W., "Determination of Profile Drag from Measurements in the Wake of a Body," *Journal of the Aeronautical Sciences*, Vol. 5, No. 6, 1938, pp. 245–249.

[10] Jones, B. M., "Measurement of Profile Drag by the Pitot-Traverse Method," Aeronautical Research Council, Rept. R&M-1688, London, 1936.

[11] Brune, G. W., "Quantitative Low-Speed Wake Survey," *Journal of Aircraft*, Vol. 31, No. 2, 1994, pp. 249–255. doi:10.2514/3.46481

[12] Zabat, M., Farascaroli, S., Browand, F., Nestlerode, M., and Baez, J., "Drag Measurements on a Platoon of Vehicles," California Partners for Advanced Transit and Highways, Inst. of Transportation Studies, Univ. of California, Berkeley Research Rept. UCB-ITS-PRR-93-27, Berkeley, CA, 1994.

[13] McArthur, J., "Aerodynamics of Wings at Low Reynolds Numbers," Ph.D. Dissertation, Dept. of Aerospace and Mechanical Engineering, Univ. of Southern California, Los Angeles, 2007.

[14] Spedding, G. R., and Hedenstrom, A., "PIV-Based Investigations of Animal Flight," *Experiments in Fluids*, Vol. 46, No. 5, 2009, pp. 749–763. doi:10.1007/s00348-008-0597-y